Colloids and Surfaces A 579 (2019) 123663

Contents lists available at ScienceDirect

Colloids and Surfaces A

journal homepage: www.elsevier.com/locate/colsurfa

pH-dependent structure, pattern and hysteresis behaviour of lipid (DMPA)-protein (BSA) monolayer complex

Bijay K. Sah, Kaushik Das, Sarathi Kundu*

Soft Nano Laboratory, Physical Sciences Division, Institute of Advanced Study in Science and Technology, Vigyan Path, Paschim Boragaon, Garchuk, Guwahati, Assam 781035, India

GRAPHICAL ABSTRACT

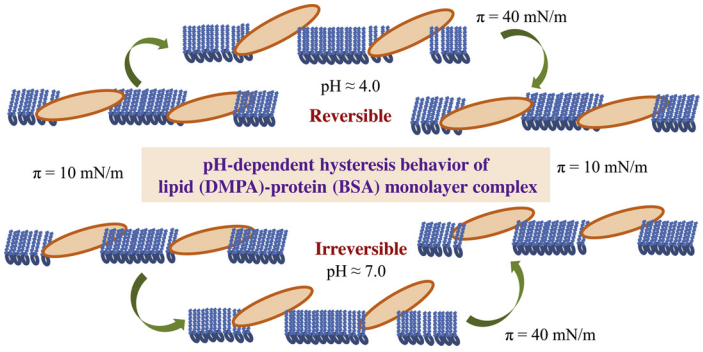

ARTICLE INFO

Keywords:
Lipid-protein complex
Monolayer pattern
Hysteresis
Out-of-plane structures
Structural modification

ABSTRACT

Understanding lipid-protein interactions in model membranes is a challenging task. Limited information exist to-date regarding the relative influence of hydrophobic and electrostatic forces on the organization of proteins inside model membranes, while these forces determine the structure of lipid-protein complexes. We measured the surface pressure (π) - molecular area (A) isotherm cycles of protein (BSA) – lipid (DMPA) mixed monolayers below and above the isoelectric point of BSA ($\approx$ 4.8). At pH $\approx$ 4.0, below the isoelectric point, BSA is positively charged, and exposes few hydrophobic groups at its surface, compression-decompression isotherms show a nearly reversible hysteresis. At pH $\approx$ 7.0, above the isoelectric point, BSA is negatively charged and more hydrophobic. At this pH, compression-decompression isotherms show an irreversible hysteresis. This behaviour indicates that the deformation of BSA molecules under pressure is reversible below the isoelectric point, while it becomes irreversible above it. X-ray reflectivity studies for protein-lipid mixed monolayers show that BSA molecules move from the zone close to water and near the lipid polar heads toward the zone occupied by their hydrocarbon tails s when surface pressure increases. Mostly the surface pressure in combinations with hydrophobic and electrostatic interactions is responsible for such structural modifications.

1. Introduction

Biological membranes play a significant role in almost every aspect of life. Many processes like molecular transport, molecular recognition and signal transduction occurs at the surface of cellular membranes. As a consequence, cell membranes as well as model membranes attracted

* Corresponding author.
E-mail address: sarathi.kundu@gmail.com (S. Kundu).

https://doi.org/10.1016/j.colsurfa.2019.123663
Received 18 March 2019; Received in revised form 9 July 2019; Accepted 10 July 2019
Available online 11 July 2019
0927-7757/

considerable attention in the past decades [1–4]. Interesting models are lipid bilayers containing proteins [5]. Protein-lipid complexes can play a crucial role in many biotechnological and medical applications such as biomimetic reconstitution of the cell-membranes [6–8] and biosensors [9]. Protein-lipid complexes are also suitable for studying the interactions among surface-active components in pulmonary surfactants [10].

Interaction of proteins with lipid bilayer can occur in different ways. They can locate in the lipid headgroup zone, partially penetrate into the hydrophobic tail zone or fully span the bilayer membrane. In most cases, membrane-embedded proteins interact with both lipid head groups and tails. A suitable matching between the hydrophobic parts of the proteins and the surrounding lipid molecules is believed to play a significant role in controlling the physicochemical properties of these membranes and the biological activity of the embedded proteins [11–17]. In particular, the variation of pH can alter the hydrophobic nature of a protein embedded in a lipid bilayer (i.e. the number of exposed hydrophobic groups at this surface), which can induce local segregation in the bilayer [13]. It has been found that the hydrophobicity of the bovine serum albumin protein (BSA) depends on the pH of the solvent. BSA becomes less hydrophobic in acidic environments (pH ≈ 3.0 or 4.0) as compared to neutral (pH ≈ 7.0) or basic environments (pH ≈ 9.0) [18]. When the pH is varied, structural modifications can occur in the bilayer. These structural changes can be detected via measurements of the mechanical, conformational and thermodynamic properties of the lipid bilayer [12,16,17,19].

It should be noted that domains' formation in monolayers can result from two different processes. In the first case, kinetic processes lead to out-of-equilibrium domains, generally when the monolayer is compressed quickly [20,21]. The interfacial activation energy can also influence the shape of the domains and their existence [22]. In the second case, equilibrium domains form as result of the interplay between their line tension and long-range dipole-dipole interactions [23,24]. In particular, the shape of the lipids can result from anisotropy in the line tension [25,26].

Two-dimensional domain-structures formed in Langmuir monolayers are of interest in the fields of optics and microelectronics for their potential applications [27]. Lipid domains are also observed in biomimetic systems, for example, in monolayers of red-blood cells lipids [28] and of bovine pulmonary surfactant membranes [29]. Domain structures formed in lipid bilayers are used to study different phases, phase transitions and properties of model membrane [30,31]. These domains also play an important role in biological processes. Formation of activator-rich domains is useful for the enhancement of enzymatic activity [32,33], and protein sorting, protein aggregation, signalling, and membrane fusion can also depend on domain formation [34,35].

In this article, the phospholipid DMPA (1, 2-dimyristoyl-sn-glycero-3-phosphate) and the globular protein BSA are used to prepare monolayers at the air-water and air-solid interfaces. We have determined the phase behavior in absence and presence of BSA at the air-water interface and at two different subphase pH values, below and above the isoelectric point of BSA. Different phases such as liquid-expanded (LE), liquid-condensed (LC) and solid (S) phases were identified along with domain formation. The corresponding structures and morphologies were also studied at the air-solid interface. The compression and decompression isotherms of DMPA-BSA complex layer were determined. Compression-decompression isotherm cycles demonstrated hysteresis. The changes in the pattern formation were investigated using Brewster's angle microscopy (BAM) during compression and after decompression. The out-of-plane structural modifications under pressure were determined with X-ray reflectivity (XRR). Monolayer structure, domain morphology and hysteresis behavior are discussed.

2. Experimental details

BSA (≥96%, catalog No. A2153) was purchased from Sigma-Aldrich. The isoelectric point of the BSA protein is ≈ 4.8 [36,37]. Phospholipid DMPA (< 99%, catalog No. 830845 P) was purchased from Avanti polar lipids. A solution containing 1 mg/ml BSA was prepared in Milli-Q water (resistivity ≈ 18.2 MΩ.cm) and a solution containing 0.5 mg/ml DMPA was prepared in chloroform (≥96%, 288306 Sigma-Aldrich). To form the mixed monolayer, a chosen amount (75 µl) of DMPA solution was carefully spread with the help of a syringe on the water surface in a Langmuir trough (Apex Instruments). After an equilibration time of 10 min, an equal volume of BSA was spread in a similar manner. The solvent used for dissolving the lipid component is chloroform and as chloroform is a non-aromatic compound so the proposed time is nearly sufficient to evaporate chloroform completely [38], however, relatively higher evaporation time is required for the aromatic solvents [39]. The surface tension changes during the spreading process were recorded using a Wilhelmy plate connected to an electro balance. DMPA monolayers were compressed and expanded at a low constant speed of ≈ 0.005 nm^2/molecule/min in order to avoid non-equilibrium effects observed during fast compression. However, since for BSA and DMPA-BSA, there were no apparent significant differences in the isotherms between 0.005 nm^2/molecule/min and higher compression speeds, the monolayers of BSA and DMPA-BSA were compressed and expanded at a constant speed of ≈ 1.54 and 0.06 nm^2/molecule/min respectively. The BAM, X-ray and other experiments were done for DMPA-BSA at the higher compression rate. All surface pressure (π) - molecular area (A) isotherm, BAM and X-ray measurements were performed at an ambient temperature of 23 °C (± 1 °C). The pH of the water subphase was adjusted at ≈ 4.0 using HCl and ≈ 7.0 using NaOH. No buffer was used in order to minimize contamination. An equilibration period of two to three hours under magnetic stirring was used to stabilize the subphase pH.

Domain patterns at different surface pressures and subphase pH were visualized by means of Brewster angle microscope (BAM) using a Nanofilm_EP4 BAM. The instrument consists of a standard 50 mW solid state laser, emitting p-polarized light at a wavelength of 658 nm. The reflected light from the surfaces is collected onto a computer controlled high quality CCD camera, which is attached to a real time frame grabber with 1392 × 1040 pixels through a 10x magnification objective. The spatial resolution of the device is ≈ 2 microns. A black wedge-shaped glass plate is placed at the bottom of the trough to reflect any light transmitted through the subphase far from the camera and to minimize the convection on the trough.

DMPA and DMPA-BSA monolayers were deposited onto solid substrates by the Langmuir-Blodgett method (LB) using only single upstroke of Si (001) substrates. Prior to the deposition, Si (001) substrates were made hydrophilic by immersion into a mixed solution of ammonium hydroxide (NH_4OH, Merck, 30%), hydrogen peroxide (H_2O_2, Merck, 30%), and Milli-Q water (H_2O: NH_4OH: H_2O_2:: 2:1:1, by volume) during 5–10 min at 100 °C. Subsequently, all the substrates were kept inside the Milli-Q water until LB deposition. Before starting the deposition, the mixed monolayers were allowed to equilibrate at the air-water surface during about 10 min. The deposition was carried at a constant speed of 2 mm/min. All depositions were performed at an ambient temperature of 23 °C (± 1 °C).

Attenuated total reflection–Fourier transform infrared (ATR-FTIR) spectroscopy was performed with the mixed monolayers on Si (001) substrates. Data was taken using a spectrophotometer (NICOLET 6700, Thermo- Fisher) within the wavelength range of 380–4000 cm^{-1} at 4 cm^{-1} resolution. Three different positions on the DMPA-BSA monolayer surface were chosen for ATR-FTIR measurements.

X-ray reflectivity (XRR) measurements of DMPA-BSA mixed monolayers on Si (001) substrates were carried out. The diffractometer (D8 Advanced, Bruker AXS) has a copper (Cu) source in a sealed tube followed by a Göbel mirror for the selection and enhancement of the Cu K_α radiation (=1.54 Å). A NaI scintillation point detector was used. Data was taken in specular conditions, i.e., the incident angle (θ) was kept equal to the reflected angle (θ), both beams both lying in the same

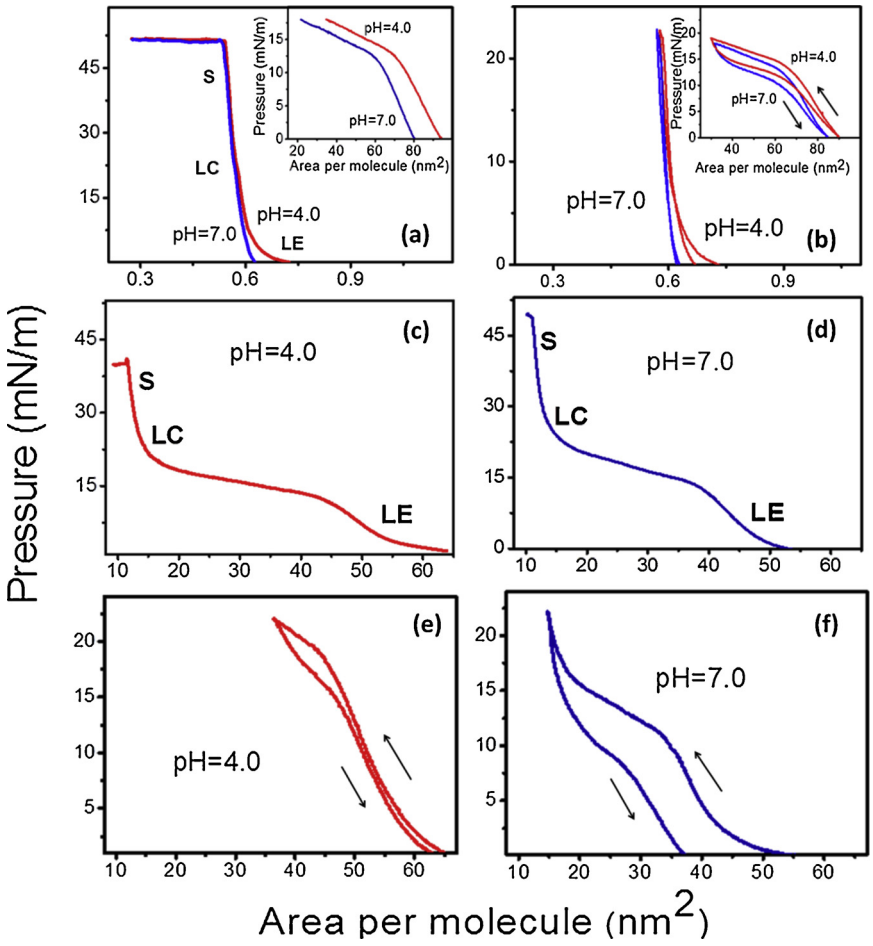

Fig. 1. Surface pressure - molecular area (π-*A*) isotherms. (a) π-*A* isotherms of DMPA at two different subphase pH values, i.e., at pH ≈ 4.0 (red line) and 7.0 (blue line). Inset: π-*A* isotherms of BSA at the same pH values. (b) Compression-decompression isotherm cycle of DMPA at pH ≈ 4.0 and 7.0 Inset: compression-decompression isotherm cycle of BSA at the same pH values. (c) π-*A* isotherms of DMPA-BSA complex at pH ≈ 4.0 (d) π-*A* isotherms of DMPA-BSA complex at pH ≈ 7.0. (e) Compression-decompression isotherm cycle of DMPA-BSA complex at pH ≈ 4.0. (f) Compression-decompression isotherm cycle of DMPA-BSA complex at pH ≈ 7.0. (For interpretation of the references to colour in this figure legend, the reader is referred to the web version of this article.)

scattering plane. Under such conditions, the vertical component of the wave-vector transfer, i.e., q_z is given by $(4\pi/\lambda)\sin\theta$. The analysis of XRR data was performed using the Parratt's formalism [40] for a stack of homogeneous layers with sharp interfaces. Both surface and interfacial roughness has been included [41,42]. The electron-density variation, i.e., the electron-density profile (EDP) is extracted from the fit [41,44], which gives in-plane (*x*–*y*) average electron density (ρ) as a function of depth (*z*) with high resolution [41–45]. Two XRR measurements were performed for each sample: the XRR profiles were nearly identical implying good reproducibility.

3. Results

Surface pressure - molecular area (π-*A*) isotherms allows the identification of phases and phase transitions in the monolayer at the air-water interface. The overall shape of the isotherm, depends upon the interaction among the monolayer forming molecules. Fig. 1a shows the π-*A* isotherm of pure DMPA monolayer at pH ≈ 4.0 (red line) and 7.0 (blue line). The corresponding inset shows π-*A* isotherms of pure BSA monolayer at the same pH values, i.e., below (pH ≈ 4.0) and above (pH ≈ 7.0) the isoelectric point (pI ≈ 4.8) of BSA in solution. Fig. 1a shows that the surface tension starts to increase when the area per molecule falls below 0.72 nm^2 at pH ≈ 4.0, and 0.62 nm^2 at pH ≈ 7.0. Fig. 1a also shows that the liquid expanded (LE) phase is transformed into a liquid condensed (LC) phase through a very narrow LE-LC phase coexistence region. Additional compression (beyond $A \approx 0.55\ nm^2$) leads to a solid phase (S). Finally, the monolayer collapses at a pressure of ≈ 51 mN/m. The compressibility value $\kappa = -(1/A)(\partial A/\partial\pi)$ decreases from ≈ 0.02 to 0.003 m/mN between LE and LC phases at the transition, both for pH ≈ 4.0 and 7.0 and drops to ≈ 0.001 m/mN in the S phase.

Fig. 1a also shows that the evolution from LE to LC is more abrupt for pH ≈ 7.0 in comparison with pH ≈ 4.0. The π-A isotherm of pure BSA (Fig. 1A inset) shows that at a given pressure, the area per molecule decreases with the increase in subphase pH, i.e., π starts to rise from ≈ 93 nm^2 at pH ≈ 4.0 to ≈ 80 nm^2 at pH ≈ 7.0. The *A* observed at pH ≈ 4.0 and 7.0 is more compared to the area per molecule (≈ 62 nm^2) observed near to the isoelectric point of BSA [46]. Similar types of results were also obtained from HSA monolayer below, above and at isoelectric point of HSA molecule as relatively less *A* is obtained at isoelectric point compared to the lower and higher pH values [47]. Fig. 1b shows the compression-decompression cycles for pure DMPA at pH ≈ 4.0 and pH ≈ 7.0 respectively, whereas its inset shows the compression-decompression cycles for pure BSA at the same pH values.

Fig. 1c and d shows the π-*A* isotherms of DMPA-BSA mixed monolayers at pH ≈ 4.0 and pH ≈ 7.0 respectively. Here 'area per molecule' actually represents the average of the area occupied by the total number of lipid and protein molecules spread on the air-water interface. The molecular weight for the DMPA-BSA complex was calculated using the formula

$$M = \frac{m_1 c_1 v_1 + m_2 c_2 v_2}{c_1 v_1 + c_2 v_2} \quad (1)$$

where m_1, m_2, c_1, c_2, v_1 and v_2 are the molecular weight, concentration and volume spread of DMPA and BSA respectively. Note that BSA is a soluble molecule. Hence, despite all the precautions taken during BSA spreading, some BSA molecules can end up in the subphase. Thus, the values for the area per molecule for the BSA and BSA-DMPA films are only upper bounds. For both pH values, 75 µl of DMPA and BSA solutions were spread on the water surface, one followed by the other. Mostly, the lateral lipid-protein interactions within the film can be

explored if both the molecules were spread at the air-water interface from the air side nearly at zero surface pressure [48]. Below the isoelectric point of BSA, i.e., at pH ≈ 4.0, the surface pressure starts to increase below A ≈ 65 nm^2 while above the isoelectric point, i.e., at pH ≈ 7.0, the pressure starts to rise below A ≈ 53 nm^2. For both pH, a plateau like feature is observed starting at nearly the same pressure ≈ 15 mN/m, but at a larger area per molecule (≈ 46 nm^2) for pH ≈ 4.0 than for pH ≈ 7.0 (≈ 38 nm^2).

The LE-LC plateau region is much wider than for the pure lipid monolayers, suggesting that the protein favours LE-LC coexistence. Upon further compression, the LC phase is transformed into a S phase before the monolayer collapses (A ≈ 10 nm^2). Fig. 1e and f shows the compression-decompression π-A isotherms for DMPA-BSA mixed monolayers at the air-water interface for pH ≈ 4.0 and 7.0 respectively. The isotherm cycle shows that for pH ≈ 4.0 the surface pressure during decompression closely follows the compression isotherm and introduces only a small amount of hysteresis. However, a more substantial hysteresis is observed for pH 7. Upon decompression, the pressure becomes zero at A ≈ 36 nm^2, while during the first compression, the pressure started to increase below A ≈ 53 nm^2. We characterized the hysteresis H by the area comprised between the compression and decompression curves; these area are ≈ 39.10 × 10^{-21} N·m and 154.82 × 10^{-21} N·m for pH ≈ 4.0 and 7.0 respectively. Note that the hysteresis depends on the barrier speed (Fig. S2 a and b): for a speed of 0.01 nm^2/molecule/min H ≈ 40.5 × 10^{-21} N·m and 100.47 × 10^{-21} N·m for pH ≈ 4.0 and 7.0 respectively.

Brewster angle microscopy is commonly used to study phase coexistence in monolayers made of lipids, proteins and their mixtures at the air-water interface under different experimental conditions [49–52]. Fig. 2 shows the BAM images of DMPA monolayers during the compression process for pH ≈ 4.0 and 7.0 and at low- and high-pressure during the first compression cycle (10 and 40 mN/m) and low-pressure value (10 mN/m) during the second compression cycle.

It is seen in the images that the DMPA domains are smaller at pH ≈ 4 than at pH ≈ 7, whatever the pressure. At low pressure, i.e., above the LE-LC coexistence region as found between 1–3.5 mN/m, the DMPA domains are homogeneously distributed over the surface, and nearly circular in shape (Fig. 2a and d), while they are more numerous, bigger and distorted at high pressure (Fig. 2b and e). In the S phase, i.e., before collapse, very dense and brighter domains are observed. The domains observed in the different phases are different from those found with other lipids like DPPC, where circular, nut-like, branched and elongated structures were observed [53–55].

After compression up to 40 mN/m, the film was allowed to expand slowly until it achieves its initial zero pressure condition and then it was compressed a second time up to 10 mN/m. During the second compression, the domains are similar to those formed during first compression (Fig. 2c). However, at pH ≈ 7.0, the domains are bigger and deformed with respect to those seen during the first compression (Fig. 2f).

Fig. 3 shows BAM images of BSA monolayers at the air-water interface for pH ≈ 4.0 (Fig. 3a–c) and for pH ≈ 7.0 (Fig. 3d–f). Fig. 3a, d shows representative images at a surface pressure of ≈ 5 mN/m, Fig. 3b, e at a surface pressure of ≈ 19 mN/m. Fig. 3c, f shows the behavior at a surface pressure of ≈ 5 mN/m during the second compression cycle. The images show that BSA forms homogeneous films, which are devoid of domains, irrespective of the pH value or the surface pressure. However, the images are brighter at higher surface pressure indicating an increase in density (and possibly thickness) of the layer. Thus, DMPA monolayers contain domain-like structures, while BSA monolayers are homogeneous under equilibrium conditions.

Fig. 4 shows the BAM images of DMPA-BSA mixed monolayers for pH ≈ 4.0 (first row) and ≈ 7.0 (second row), at three different surface pressures π ≈ 10 mN/m, π ≈ 40 mN/m and again π ≈ 10 mN/m during the second compression. The images obtained at pH ≈ 4.0 show the formation of broad network-like structures with narrow channels spanning between them. Globular-like white spots of variable size appear in the majority of the images and located close to the domain centres, probably resulting from protein aggregation (Fig. 4a). At higher pressure, the domains come closer to each other, while the aggregates remain intact nearly at the center of the domains. During the second compression cycle, the layers resemble to those obtained at the same pressure during first compression cycle. The aggregates maintain their arrangement (Fig. 4c). At pH ≈ 7.0, during the first compression cycle, less aggregates form, while the domains are slightly larger and denser (Fig. 4d-e-f).

Increasing the surface pressure in the films may induce internal structural changes in the BSA protein's conformation. This possibility was investigated using ATR-FTIR. Fig. 5 shows the amide-bond ATR-FTIR spectra of BSA in the BSA-DMPA mixed monolayer for **(a)** pH ≈ 4.0 and **(b)** pH ≈ 7.0. The amide-I band (1700–1600 cm^{-1}) is considered to be the most sensitive spectral region for obtaining secondary structure information of proteins [56]. Within the amide-I band of the BSA-DMPA film, 14 peaks are detected. Peaks found at 1623, 1627,

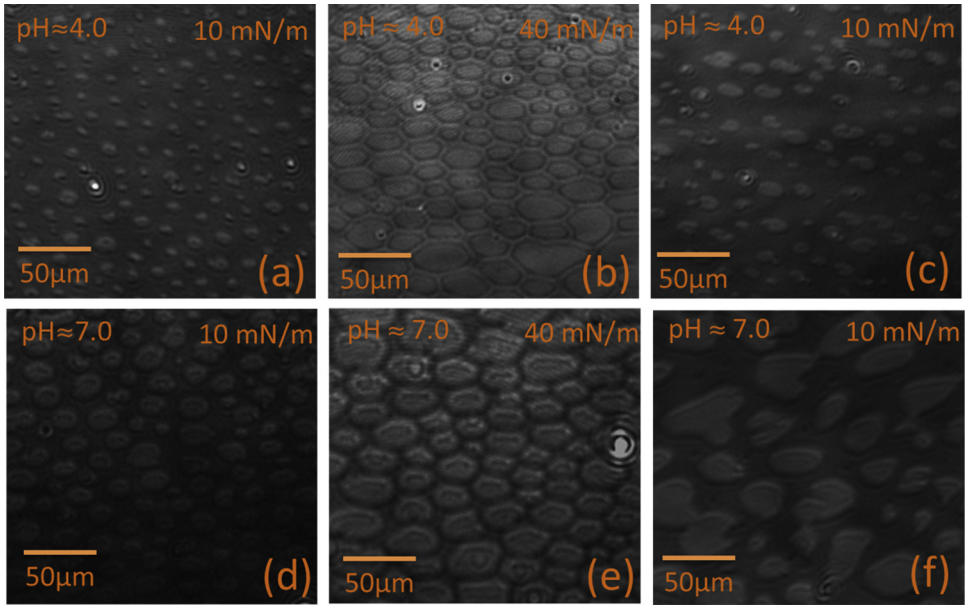

Fig. 2. Representative BAM images of a DMPA film during the compression process. (a–c): Images at subphase pH ≈ 4.0. (d–e): Images at subphase pH ≈ 7.0. The first column (a, d) shows the behavior of the DMPA monolayer at low pressure (10 mN/m). The second column (b, e) shows the behavior of the DMPA monolayer at high pressure (40 mN/m). The third column (c, f) shows the behavior of the DMPA monolayer at low pressure (10 mN/m) during the second compression cycle.

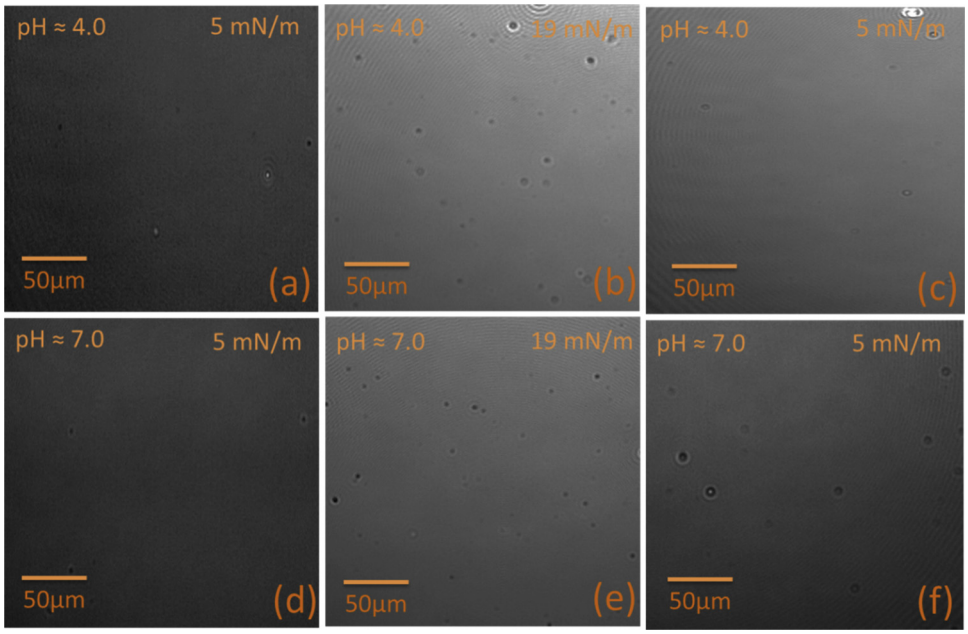

Fig. 3. BAM images of BSA monolayers during first compression at lower (π = 5 mN/m) and higher (π = 19 mN/m) surface pressures are shown in first and second column, while third column is for the same film at lower (π = 5 mN/m) pressure during second compression at two different pH values, i.e., at ≈ 4.0 (a, b and c) and 7.0 (d, e and f).

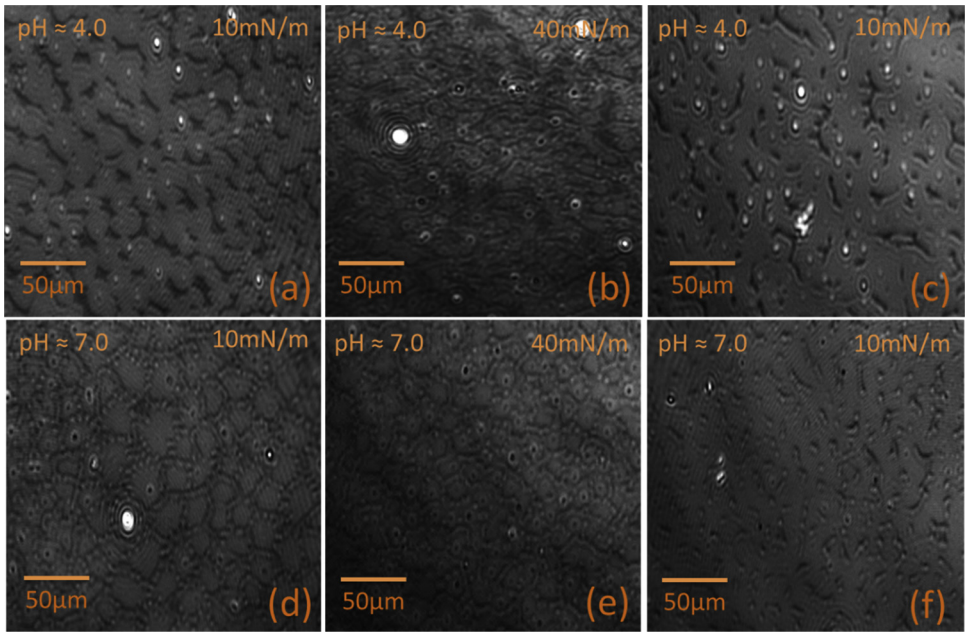

Fig. 4. BAM images of DMPA-BSA mixed monolayers during the first compression at low ($\pi \approx$ 10 mN/m) and high ($\pi \approx$ 40 mN/m) surface tensions are shown in first and second column, while third column is for the same film at low ($\pi \approx$ 10 mN/m) surface pressure during the second compression cycle at two different pH values, i.e., at ≈ 4.0 (a, b and c) and 7.0 (d, e and f).

1636 and 1697 cm^{-1} are related with beta sheet and the peaks found at 1669, 1674, 1684 and 1687 cm^{-1} are related to beta turn. Other peaks observed at 1603, 1607, 1615, 1646, 1654 and 1662 cm^{-1} correspond to side chain vibration, intermolecular beta strand, intramolecular beta strand, random coil, alpha helix and 3_{10} helix respectively [56]. To study the area under the peak, three peaks are analysed namely beta sheet (1636), random coil (1646) and alpha helix (1654). The ratio of the three peaks to 1654 cm^{-1} is also calculated for both the pH. Area under the peaks and peak ratio values are tabulated in Table 1. For pH ≈ 4.0, at π = 10 mN/m during the first compression the area under the peaks are 0.17 ± 0.015, 0.22 ± 0.020 and 0.24 ± 0.015 a.u., whereas for higher pressure ($\pi \approx$ 40 mN/m) the calculated area is 0.23 ± 0.010, 0.25 ± 0.005 and 0.26 ± 0.005 a.u. respectively. Similarly, at low surface pressure ($\pi \approx$ 10 mN/m) during the second compression cycle, the areas under the peaks are 0.16 ± 0.005, 0.21 ± 0.010 and 0.22 ± 0.005 a.u. respectively. The ratios of the 1654 cm^{-1} peak to the area under the other two peaks at 10 and 40 mN/m during the first compression are 1.41 ± 0.290 and 1.09 ± 0.296, and 1.13 ± 0.137 and 1.04 ± 0.080 respectively. However during second compression at 10 mN/m the corresponding ratios are 1.38 ± 0.149 and 1.04 ± 0.148. On the other hand, for pH ≈ 7.0 and low surface pressure ($\pi \approx$ 10 mN/m) during the first compression cycle, the observed areas corresponding to the above mentioned three peaks are 0.19 ± 0.010, 0.25 ± 0.010 and 0.25 ± 0.005 a.u. respectively. At higher surface pressure (π = 40 mN/m) the areas observed are 0.19 ± 0.015, 0.24 ± 0.020 and 0.25 ± 0.015 a.u. Similarly, at $\pi \approx$ 10 mN/m during the second compression cycle the calculated areas under the peaks are 0.16 ± 0.005, 0.21 ± 0.010 and 0.22 ± 0.010 a.u. respectively. The ratios of the 1654 cm^{-1} peak to the area under the other two peaks at 10 and 40 mN/m during first compression are 1.32 ± 0.195 and 1.00 ± 0.120, and 1.32 ± 0.284 and 1.04 ± 0.300 respectively. However during second compression at 10 mN/m the corresponding ratios are 1.38 ± 0.211 and 1.04 ± 0.195. Thus, we see that all of the secondary structures of BSA

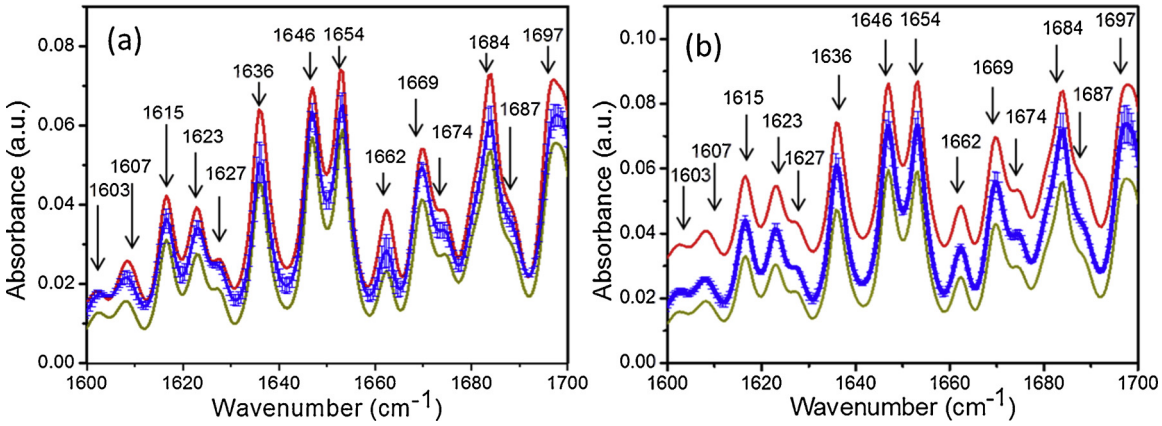

Fig. 5. ATR-FTIR spectra of Amide-I band of BSA obtained from DMPA-BSA mixed films at (A) pH ≈ 4.0 and (B) pH ≈ 7.0, for two different pressure conditions, i.e., at 10 mN/m (blue) and 40 mN/m (red) during the first compression and again at 10 mN/m (dark yellow) during the second compression. Arrows indicate the corresponding peak positions. For clarity error bar is included only for the middle curve. (For interpretation of the references to colour in this figure legend, the reader is referred to the web version of this article.)

Table 1
Peak ratios of 1636 and 1646 cm^{-1} to 1654 cm^{-1} and area under the peaks 1636, 1646 and 1654 cm^{-1} for pH ≈ 4.0 and 7.0 respectively.

pH	π (mN/m)	A_{1654}/A_{1636}	A_{1654}/A_{1646}	A_{1636} (a.u.)	A_{1646} (a.u.)	A_{1654} (a.u.)
4	10	1.41 ± 0.290	1.09 ± 0.296	0.17 ± 0.015	0.22 ± 0.020	0.24 ± 0.015
	40	1.13 ± 0.137	1.04 ± 0.080	0.23 ± 0.010	0.25 ± 0.005	0.26 ± 0.005
	10	1.38 ± 0.149	1.04 ± 0.148	0.16 ± 0.005	0.21 ± 0.010	0.22 ± 0.005
7	10	1.32 ± 0.195	1.00 ± 0.120	0.19 ± 0.010	0.25 ± 0.010	0.25 ± 0.005
	40	1.32 ± 0.284	1.04 ± 0.300	0.19 ± 0.015	0.24 ± 0.020	0.25 ± 0.015
	10	1.38 ± 0.211	1.04 ± 0.195	0.16 ± 0.005	0.21 ± 0.010	0.22 ± 0.010

are present in the mixed monolayers for both pH conditions but their relative amounts are different, which is the signature of pH effects at the air-water interface [57,58]. The values obtained from peak ratios show that at pH ≈ 4.0, the compression results in slight modifications of the protein secondary structures, almost fully reversible. In contrast, at pH ≈ 7.0 there is hardly any modification with pressure and eventual differences in secondary structure are not observable.

To obtain the out-of-plane XRR profile at different surface pressure conditions, monolayers were deposited on the hydrophilic silicon Si (001) substrates. Pure DMPA monolayers were deposited at π ≈ 20 mN/m for two different pH conditions (pH ≈ 4.0 and 7.0). The reflectivity data and the corresponding fitted curves are shown in the Fig. S1, whereas the EDPs obtained are shown in the inset of the corresponding figure. EDPs obtained from the DMPA-BSA mixed monolayers are also included in Fig. S1 for comparison. Relatively higher electron density and thickness obtained from the mixed monolayers confirms the presence of BSA in the DMPA-BSA mixed monolayers.

X-ray reflectivity data (open circles) and the corresponding fitted lines obtained from the DMPA-BSA mixed monolayers for pH ≈ 4.0 and 7.0 are shown in Figs. 6a and 7 arespectively. From the EDPs shown in Fig. 6b it is clear at pH ≈ 4.0, the electron density slightly increases away from the film surface. This result probably indicates that the lipid molecules become less tilted at higher surface pressure. However, as is discussed below, this can also indicate a longitudinal transfer of the BSA molecules or slight tilting of the BSA molecules from the air-water interface. Further increase of the pressure to π ≈ 40 mN/m the EDP shows the formation of a second peak in the EDP spectra at z ≈ 26 Å (el/Å^3 ≈ 0.58, Fig. 6b, blue line). The formation of this peak probably indicates that some BSA molecules have been driven slightly towards the lipid hydrophobic tail part or air-side as shown in the cartoon of Fig. 8a. However, the formation of the second peak in the EDP spectra at z ≈ 26 Å may arise due to the structural changes in the BSA molecules as detected by the ATR-FTIR results. The relatively lower density near the substrate surface (≈ 0.82 el/Å^3) is obtained from the lipid headgroups and BSA. Interestingly, the EDP of the BSA-DMPA film at π ≈ 10 mN/m during the second compression cycle closely resembles the EDP result at the same surface pressure value during the first compression cycle. This result suggests that the film approximately recovered its structure, which is in agreement with the BAM images, the ATR-FTIR and isotherm results.

The EDP spectrum at pH 7.0 at the low surface pressure value (10 mN/m) and during the first compression cycle shows a small peak at z = 26 Å (Fig. 7b, black line). This bump probably results from the presence of BSA molecules inside the hydrocarbon tails. At π ≈ 20 mN/m the electron density peak at 25 Å above the substrate surface increases (density ≈ 0.60 el/Å^3). This result suggests that increasing the surface pressure and the compactness of the film caused more BSA molecules to shift to the hydrophobic tail phase of the film. With further increase in the surface pressure (π ≈ 20 mN/m) the same peak at z = 25 Å further increases, indicating even a larger buildup of BSA molecules pool in the hydrophobic part of the film. In addition, a large increase in the electron density next to the substrate surface is observed. It is hard to explain these results. The mechanism of BSA pool build up in the hydrophobic phase of the film is illustrated in Fig. 8b. During the second compression cycle, at the low surface pressure value (π ≈ 10 mN/m), the EDP reaches a zero electron density value approximately at the same z-value than during the first compression cycle at the same surface pressure. However, the integral of the electron density over the z-direction is larger than the one during the first compression cycle. The fact that the electron density peak at z = 25 Å during the second compression cycle is larger than during the first compression cycle suggests that the BSA molecules, once lifted from the air-water interfaces, find it difficult to restore to their initial position. Thus, a long-lived structural deformation is obtained in the DMPA-BSA film, which results in hysteresis of the isotherm. A similar result was not observed at pH 4.0 due to the higher hydrophilicity of the BSA molecules at this pH value.

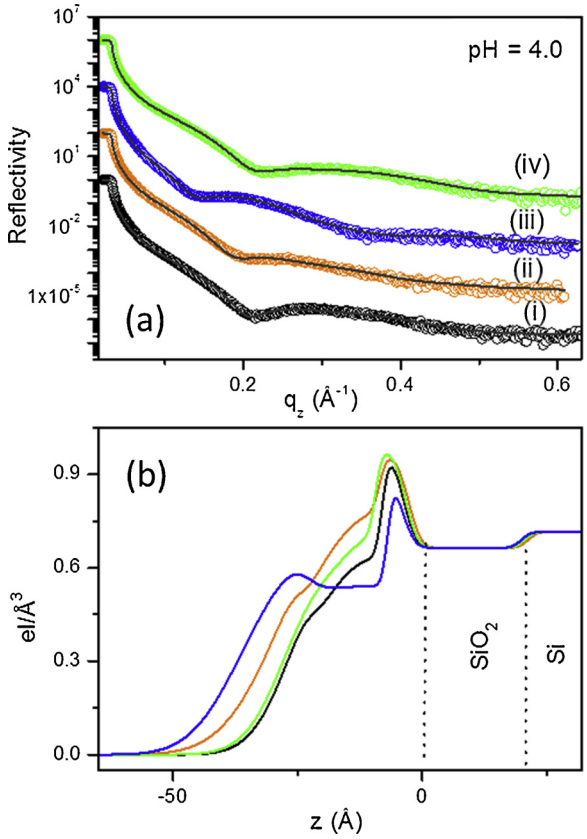

Fig. 6. (a) X-ray reflectivity data (circles) and the corresponding fitted curves (solid lines) obtained from the DMPA-BSA mixed monolayers at (i) 10 mN/m (ii) 20 mN/m, (iii) 40 mN/m during first compression, and again at (iv) 10 mN/m during second compression of the DMPA-BSA monolayer at pH ≈ 4.0. Reflectivity data and fitted curves are shifted vertically for clarity. (b) Corresponding electron density profiles extracted from the fitting of the reflectivity data. Maximum error obtained in electron density is 3–5% for each EDP.

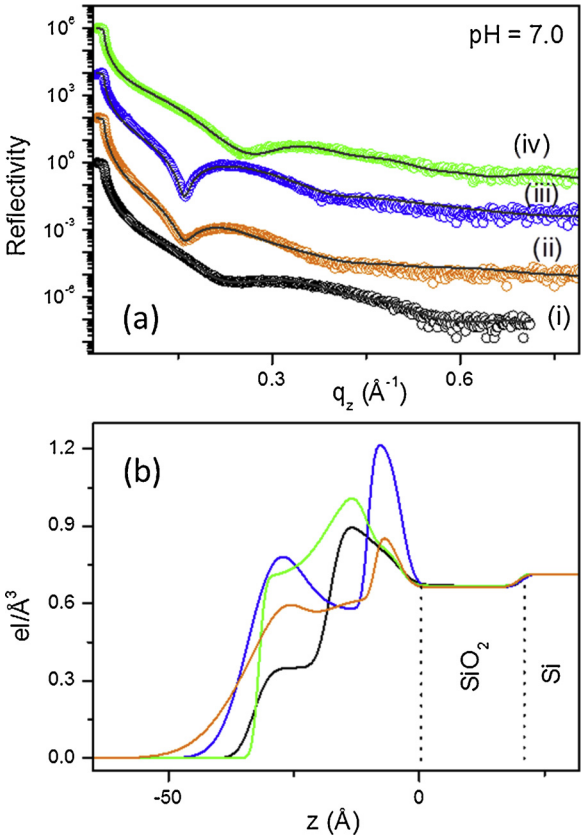

Fig. 7. (a) X-ray reflectivity data (circle) and the corresponding fitted curves (solid line) obtained from the DMPA-BSA complex films at (i) 10 mN/m (ii) 20 mN/m, (iii) 40 mN/m during first compression, and again at (iv) 10 mN/m during second compression of the BSA monolayer at pH ≈ 7.0. Reflectivity data and fitted curves are shifted vertically for clarity. (b) Corresponding electron density profiles extracted from the fitting of the reflectivity data. Maximum error obtained in electron density is 3–5% for each EDP.

4. Discussion

BSA has a heart-shaped structure at natural pH in aqueous solutions that is called normal or 'N' shape [59]. More recent results using small angle X-ray and neutron scattering study found that BSA has oblate ellipsoid like structure with radii of $a \times b \times b \approx 9\,Å \times 39\,Å \times 39\,Å$ [60,61]. Below pH ≈ 4.0, BSA is deformed into a structure called fast migrating form ('F' form) while below pH ≈ 3.5, its preferred structure is called expanded form [59]. Above pH ≈ 8.0, the lower energy state of the protein is a called basic form ('B' from). This structure is transformed with time to an 'aged' form [59]. Thus, the BSA structure remains nearly unaltered between pH ≈ 4.0 to 8.0. X-ray scattering also confirms that the BSA native structure is preserved between pH ≈ 4.0 to 9.0 [59]. However, the surrounding environment can alter the protein surface hydrophobicity, even without changing the overall structure of the protein. Probably the change in subphase pH from acidic to neutral value can cause some conformational changes in proteins [58], which are responsible for the change of hydrophobicity.

To study the phase behaviour and domain patterns in a lipid monolayer, DMPA was also used by other groups; different phases and domains in coexistence regions were observed [62,63]. The shape and size of the domains changes in the presence of other components like proteins [64,65]. While positive line tensions between the domains and the two-dimensional continuous phase favours circular shapes, dipole-dipole interactions favours branched shapes. The observed structure, shape and size of the domains result from the combination of these forces [66]. The hysteresis evidenced from the compression-decompression isotherm cycles of DMPA-BSA mixed monolayers is reversible at pH ≈ 4.0 and irreversible at pH ≈ 7.0. Similar results are also obtained from the ATR-FTIR spectra study of the Amide-I band of BSA at the lower compression and decompression speed (0.01 nm^2/molecule/min), as shown in Fig. S2a, b. Small structural variation are seen during the compression cycle at pH ≈ 4.0 but negligible ones at pH ≈ 7.0.

Out-of-plane profiles obtained from the EDPs spectra at pH ≈ 4.0 suggest that BSA molecules are located at air-water interface at low surface pressure. However, as the pressure is slowly increased the molecules get shifted from the air-water interface to the hydrocarbon tail phase. In addition, ATR-FTIR spectra at the same pH value suggest that at higher surface pressure some internal structural modifications of the BSA molecules occur during the compression process. The fact that at pH ≈ 4.0 the BSA molecules are somewhat hydrophilic, enable them to relocate at the air-water interface as the pressure is decreased during the decompression process. On the other hand, BSA molecules are present in the hydrocarbon tail zone at pH ≈ 7.0 already at low surface pressure. Since the BSA molecules are slightly hydrophobic at pH ≈ 7.0, they will tend to partition between the more hydrophilic phase of the monolayer and the more hydrophobic one. As the pressure increases at this pH, more BSA molecules migrate to the hydrocarbon tail zone. The number of BSA molecules migrating to the hydrocarbon tail zone is greater at pH ≈ 7.0 than at pH ≈ 4.0. When BSA molecules locate into the hydrophobic lipid tail zone, they do not easily come back close to the lipid polar heads during decompression. For this reason the mixed monolayer shows irreversible hysteresis (on the time scale of the

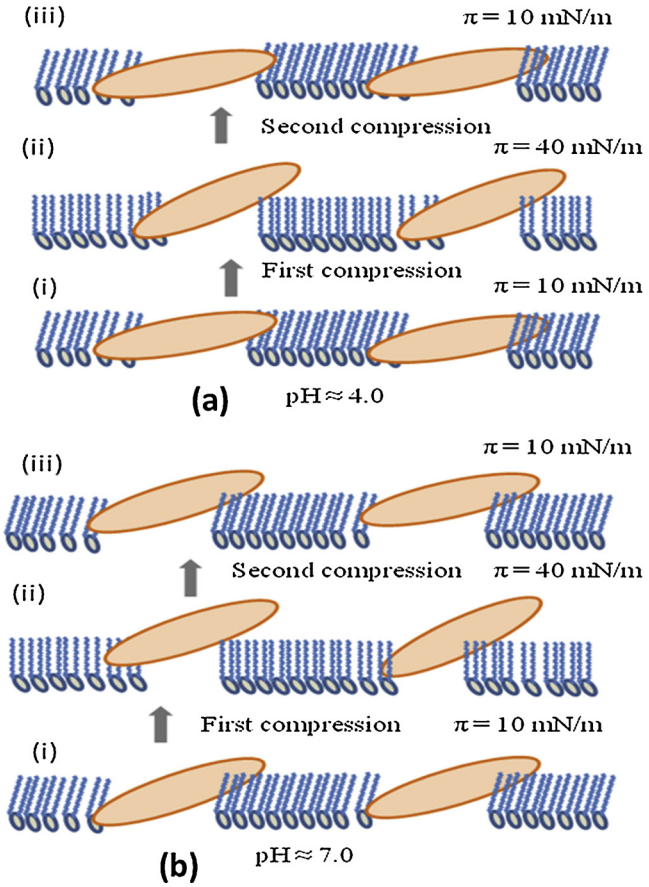

Fig. 8. Schematic representation of structural modifications for lower (10 mN/m) and higher (40 mN/m) surface pressure at (a) pH ≈ 4.0 and (b) pH ≈ 7.0. DMPA-BSA mixed monolayer gets a modification at higher surface pressure.

experiment) at pH ≈ 7.0. Thus, it can be concluded from the π-*A* isotherms, BAM, FTIR and XRR studies that probably small conformational changes of BSA molecules modify the surface hydrophobicity at the air-water interface depending on the subphase pH [18,58]. As a consequence, the protein-lipid mixed monolayers formed at the air-water interface show reversible/irreversible structural transformations below/above the isoelectric point of BSA protein.

5. Conclusions

Studies on the surface pressure of lipid-protein (DMPA-BSA) mixed monolayers at the air-water interface, at two different subphase pH conditions (pH ≈ 4.0 and 7.0), i.e., below and above the isoelectric point of BSA (≈ 4.8), were performed. The hydrophobic and electrostatic nature of BSA, which is related with the BSA conformational change in acidic conditions, is thus crucial for the almost reversible behavior of the BSA-DMPA monolayer at pH ≈ 4.0. X-ray scattering shows that when compressed protein-lipid monolayers are deposited on silicon substrates, shifting of the BSA molecules from the air-water interface to the hydrocarbon tail zone occur. However, during the decompression process, BSA molecules retain both their initial location at the air-water interface and their structural conformation. In contrast, if the pH is above the isoelectric point of BSA, hardly any internal conformational changes occur in the BSA molecules structure. In addition, at this pH value, a large portion of the BSA molecules retain their position in the lipid tail zone during the decompression process after shifting location during the compression process. Such localization of the BSA molecules results in a larger hysteresis behavior of the isotherm at pH ≈ 7.0 than at pH ≈ 4.0. This work thus shows that in addition with surface pressure, subphase pH also plays a significant role in determining the mutual lipid-protein interactions which modifies the physiochemical properties of the lipid-protein membranes.

Conflicts of Interest

None.

Acknowledgements

The work is supported by Department of Science and Technology (DST), Nano Mission, Govt. of India (Grant No. SR/NM/NS-1035/2013(G)). B.K.S. acknowledges Council for Scientific and Industrial Research (CSIR), Govt. of India for CSIR-SRF fellowship (Grant No: 09/835(0027)/2019-EMR-I). Authors acknowledge Prof. Dominique Langevin, Universite Paris Sud, France for her kind support in overall modification of the manuscript.

Appendix A. Supplementary data

Supplementary material related to this article can be found, in the online version, at doi:https://doi.org/10.1016/j.colsurfa.2019.123663.

References

[1] T. Hianik, V.I. Passechnik, Bilayer Lipid Membranes: Structure and Mechanical Properties, Kluwer Academic Publishers, Netherlands, 1995.
[2] E.J. Choi, M.D. Foster, The role of specific binding in human serum albumin adsorption to self-assembled monolayers, Langmuir 18 (2) (2002) 557–561.
[3] D. Stamou, C. Duschl, E. Delamarche, H. Vogel, Self-assembled microarrays of attoliter molecular vessels, Angew. Chem. 115 (45) (2003) 5738–5741.
[4] D. Falconnet, A. Koenig, F. Assi, M.A. Textor, Combined photolithographic and molecular-assembly approach to produce functional micropatterns for applications in the biosciences, Adv. Funct. Mater. 14 (8) (2004) 749–756.
[5] N.F. Crawford, R.M. Leblanc, Serum albumin in 2D: a Langmuir monolayer approach, Adv. Colloid Interface Sci. 207 (2014) 131–138.
[6] A.B. Serfis, R. Katzenberger, K. Williams, N. Tran, Association of blood clotting factors I and VII with phospholipid monolayers at the air–water interface, J. Colloid Interface Sci. 215 (1999) 356–363.
[7] J.A. Castleden, Phospholipid cell-membrane models, J. Pharmacol. Sci. 58 (1969) 149–165.
[8] D.G. Zhu, M.C. Petty, H.H. Ancelin, J. Yarwood, On the formation of Langmuir-Blodgett films containing enzymes, Thin Solid Films 176 (1) (1989) 151–156.
[9] Y. Okahata, T. Tsuruta, K. Ijiro, K. Ariga, Preparations of Langmuir-Blodgett films of enzyme-lipid complexes: a glucose sensor membrane, Thin Solid Films 180 (1989) 65–72.
[10] E. Sackmann, Supported membranes: scientific and practical applications, Science 271 (1996) 43–48.
[11] J.R. Abney, J.C. Owicki, Theories of Protein-Lipid and protein-protein Interactions in Membranes, Elsevier science publisher, Amsterdam, 1985, pp. 1–60.
[12] M. Bloom, E. Evans, O.G. Mouritsen, Physical properties of the fluid lipid-bilayer component of cell membranes: a perspective, Q. Rev. Biophys. 24 (3) (1991) 293–397.
[13] E. Sackmann, Physical Basis of Trigger Processes and Membrane Structures, Academic Press, New York, 1984, pp. 105–143.
[14] J. Riegler, H. Mohwald, Elastic interactions of photosynthetic reaction center proteins affecting phase transitions and protein distributions, Biophys. J. 49 (1986) 1111–1118.
[15] J. Peschke, J. Riegler, H. Mohwald, Quantitative analysis of membrane distortions induced by mismatch of protein and lipid hydrophobic thickness, Biophys. J. 14 (7) (1987) 385–391.
[16] Y. Zhang, R.N.A.H. Lewis, R.S. Hodges, R.N. McElhaney, Interaction of a peptide model of a hydrophobic transmembrane. alpha.-helical segment of a membrane protein with phosphatidylcholine bilayers: differential scanning calorimetric and FTIR spectroscopic studies, Biochemistry 31 (46) (1992) 11579–11588.
[17] J.R. Elliott, D. Needham, J.P. Dilger, D.A. Haydon, The effects of bilayer thickness and tension on gramicidin single-channel lifetime, Biochim. Biophys. Acta 735 (1) (1983) 95–103.
[18] N. Alizadeh-Pasdar, E.C.Y. Li-Chan, Comparison of protein surface hydrophobicity measured at various pH values using three different fluorescent probes, J. Agric. Food Chem. 48 (2) (2000) 328–334.
[19] F. Jahnig, H. Vogel, L. Best, Unifying description of the effect of membrane proteins on lipid order. Verification for the melittin/dimyristoylphosphatidylcholine system, Biochemistry 21 (26) (1982) 6790–6798.
[20] A. Flores, E. Corvera-Poiré, C. Garza, R. Castillo, Pattern formation and morphology evolution in Langmuir Monolayers, J. Phys. Chem. B 110 (10) (2006) 4824–4835.
[21] A. Miller, H. Möhwald, Diffusion limited growth of crystalline domains in phospholipid monolayers, J. Chem. Phys. 86 (7) (1987) 4258–4265.

[22] L. Reinhard, D. Rumiana, Domains in membranes and vesicles, J. Phys. Condens. Matter 15 (2003) S31–S45.
[23] K.Y.C. Lee, H.M. McConnell, Quantized symmetry of liquid monolayer domains, J. Phys. Chem. 97 (37) (1993) 9532–9539.
[24] H.A. Stone, H.M. McConnell, Hydrodynamics of quantized shape transitions in lipid domains, Proc. R. Soc. London, Ser. A 448 (1995).
[25] V.D. Gordon, P.A. Beales, Z. Zhao, C. Blake, F.C. MacKintosh, P.D. Olmsted, M.E. Cates, S.U. Egelhaaf, W.C.K. Poon, Lipid organization and the morphology of solid-like domains in phase-separating binary lipid membranes, J. Phys. Condens. Matter 18 (32) (2006) L415–L420.
[26] J. Korlach, P. Schwille, W.W. Webb, G.W. Feigenson, Characterization of lipid bilayer phases by confocal microscopy and fluorescence correlation spectroscopy, Proc. Natl. Acad. Sci. U. S. A. 96 (15) (1999) 8461–8466.
[27] M.C. Petty, Langmuir-Blodgett films: An introduction. Cambridge University Press, Cambridge, 1996.
[28] S.L. Keller, W.H. Pitcher III, W.H. Huestis, H.M. McConnell, Red blood cell lipids form immiscible liquids, Phys. Rev. Lett. 81 (22) (1998) 5019–5022.
[29] J.B. de la Serna, J. Perez-Gil, A.C. Simonsen, L.A. Bagatolli, Direct observation of the coexistence of two fluid phases in native pulmonary surfactant membranes at physiological temperatures, J. Biol. Chem. 279 (2004) 40715–40722.
[30] G.W. Feigenson, Phase diagrams and lipid domains in multicomponent lipid bilayer mixtures, Biochim. Biophys. Acta 1788 (2009) 47–52.
[31] I. Plasencia, L. Norlen, L.A. Bagatolli, Direct visualization of lipid domains in human skin stratum corneum's lipid membranes: effect of pH and temperature, Biophys. J. 93 (9) (2007) 3142–3155.
[32] A.R.G. Dibble, A.K. Hinderliter, J.J. Sando, R.L. Biltonen, Lipid lateral heterogeneity in phosphatidylcholine-phosphatidylserinediacylglycerol vesicles and its influence on protein kinase C activation, Biophys. J. 71 (4) (1996) 1877–1890.
[33] O.P. Karlsson, M. Rytomaa, A. Dahlqvist, P.K.J. Kinnunen, A. Wieslander, Correlation between bilayer lipid dynamics and activity of diglucosyldiacylglycerol synthase from Acholeplasma laidlawii membranes, Biochemistry 35 (31) (1996) 10094–10102.
[34] K. Simons, E. Ikonen, Functional rafts in cell membrane, Nature 387 (1997) 569–572.
[35] M. Edidin, Lipid microdomains in cell surface membranes, Curr. Opin. Struct. Biol. 7 (4) (1997) 528–532.
[36] D. Malamud, J.W. Drysdale, Isoelectric points of proteins: a table, Anal. Biochem. 86 (2) (1987) 620–647.
[37] W.J. Gelsema, C.Ld. Ligny, N.Gvd Veen, Isoelectric focusing as a method for the characterization of ampholytes : III. Isoelectric points of carrier ampholytes and dissociation constants of some carboxylic acids and alkyl-substituted ammonium ions in sucrose-water, glycerol-water and ethylene glycol-water mixtures, J. Chromatogr. A 154 (1978) 161–174.
[38] S. Steffens, J. Oldendorf, G. Haufe, H.-J. Galla, Organized collapse structures in mixtures of chiral ethyl 2-Azido-4-fluoro-3-hydroxystearates, Langmuir (22) (2006) 1428–1435.
[39] J. Orbulescu, R.M. Leblanc, Importance of the spreading solvent evaporation time in langmuir monolayers, J. Phys. Chem. C 113 (2009) 5313–5315.
[40] L.G. Parratt, Surface studies of solids by total reflection of X-Rays, Phys. Rev. 95 (1954) 359–369.
[41] J. Daillant, A. Gibaud, X-Ray and Neutron Reflectivity: Principles and Applications, Springer, Berlin, 2009.
[42] M. Tolan, X-Ray Scattering From Soft Matter Thin Films, Springer, Berlin, 1999.
[43] J.K. Basu, M.K. Sanyal, Ordering and growth of Langmuir–blodgett films: X-ray scattering studies, Phys. Rep. 363 (1) (2002) 1–84.
[44] S. Kundu, A. Datta, M.K. Sanyal, J. Daillant, D. Luzet, C. Blot, B. Struth, Growth of bimolecular films of three-tailed amphiphiles, Phys. Rev. E 73 (6) (2006) 061602-1-0616026.
[45] S. Kundu, A. Datta, S. Hazra, Effect of metal ions on monolayer collapses, Langmuir 21 (13) (2005) 5894–5900.
[46] B.K. Sah, S. Kundu, Modification of hysteresis behaviors of protein monolayer and the corresponding structures with the variation of protein surface charges, Colloids Surf. B Biointerfaces 159 (2017) 696–704.
[47] N.F. Crawford, R.M. Leblanc, Serum albumin in 2D : A Langmuir monolayer approach, Adv. Colloid Interface Sci. 207 (2014) 131–138.
[48] W.R. Glomm, Sondre Volden, Ø. Halskau Jr, M.H.G. Ese, Same system-different results: the importance of protein-introduction protocols in langmuir-monolayer studies of lipid-protein interactions, Anal. Chem. 81 (2009) 3042–3050.
[49] W.R. Glomm, M.H.G. Ese, S. Volden, C. Pitois, A. Hult, Europium (III)-cored fluorinated dendrimers at the air–water surface, Colloid Surf. A: Physicochem. Eng. Asp. 299 (1-3) (2007) 186–197.
[50] Q. He, J.B. Li, Hydrolysis characterization of phospholipid monolayers catalyzed by different phospholipases at the air–water interface, Adv. Colloid Interface Sci. 131 (2007) 91–98.
[51] G. Sui, M. Micic, Q. Huo, R.M. Leblanc, Studies of a novel polymerizable amphiphilic dendrimer, Colloid Surf., A: Physicochem. Eng. Asp. 171 (1–3) (2000) 185–197.
[52] O. Brandal, T. Viitala, J. Sjoblom, Compression isotherms and morphological characteristics of pure and mixed langmuir monolayers of C80 isoprenoid tetraacids and a C18 monoacid, J. Dispersion Sci. Technol. 28 (1) (2007) 95–106.
[53] A. Flores, P. Ize, S. Ramos, R. Castillo, The dioctadecylamine monolayer: Textures, phase transitions, and dendritic growth, J. Chem. Phys. 119 (2003) 5644–5653.
[54] A.J. Sheridan, J.M. Slater, T. Arnold, R.A. Campbell, K.C. Thompson, Changes to DPPC domain structure in the presence of carbon nanoparticles, Langmuir 33 (2017) 10374–10384.
[55] K. Kim, S.Q. Choi, J.A. Zasadzinski, T.M. Squires, Interfacial microrheology of DPPC monolayers at the air–water interface, Soft Matter 7 (2011) 7782–7789.
[56] J. Kong, S. Yu, Fourier transform infrared spectroscopic analysis of protein secondary structures, Acta Biochim. Biophys. Sin. 39 (2007) 549–559.
[57] K. Das, S. Kundu, Adsorption and conformation variation of BSA protein with the size variation of the metallic nanoparticles in LB film, Colloid Surf. A: Physicochem. Eng. Asp. 468 (2015) 56–61.
[58] D.C. Carter, J.X. Ho, Structure of serum albumin, Adv. Protein Chem. 45 (1994) 153–203.
[59] L.R.S. Barbosa, M.G. Ortore, F. Spinozzi, P. Mariani, S. Bernstorff, R. Itri, The importance of protein-protein interactions on the pH-Induced conformational changes of bovine serum albumin: a small-angle X-Ray scattering study, Biophys. J. 98 (1) (2010) 147–157.
[60] F. Zhang, F. Roosen-Runge, M.W.A. Skoda, R.M.J. Jacobs, M. Wolf, P. Callow, H. Frielinghaus, V. Pipich, S. Prévost, F. Schreiber, Hydration and interactions in protein solutions containing concentrated electrolytes studied by small-angle scattering, Phys. Chem. Chem. Phys. 14 (7) (2012) 2483–2493.
[61] S. Kundu, K. Das, V.K. Aswal, Modification of attractive and repulsive interactions among proteins in solution due to the presence of mono-, di- and tri-valent ions, Chem. Phys. Lett. 578 (2013) 115–119.
[62] M. Lösche, H. Möhwald, Impurity controlled phase transitions of phospholipid monolayers, Eur. Biophys. J. 11 (1) (1984) 35–42.
[63] D. Vaknin, P. Krüger, M. Lösche, Anomalous X-Ray reflectivity characterization of ion distribution at biomimetic membranes, Phys. Rev. Lett. 90 (17) (2003) 178102-1-178102-4.
[64] J.P. Hagen, H.M. McConnell, Critical pressures in multicomponent lipid monolayers, Biochim. Biophys. Acta 1280 (2) (1996) 169–172.
[65] T. Yamamoto, T. Manaka, M. Iwamoto, The interacting electrostatic charge model on the shape formation of monolayer domains as the air–water interface comprised of tilted dipoles with orientational deformation, Thin Solid Films 516 (9) (2008) 2660–2665.
[66] Y. Hu, K. Meleson, J. Israelachvili, Thermodynamic equilibrium of domains in a two-component Langmuir monolayer, Biophys. J. 91 (2) (2006) 444–453.